

Effect of Ferroelectric Polarization on Ionic Transport and Resistance Degradation in BaTiO₃ by Phase-Field Approach

Ye Cao,^{‡,†} Jie Shen,[§] Clive Randall,[‡] and Long-Qing Chen[‡]

[‡]Department of Materials Science and Engineering, The Pennsylvania State University, University Park, Pennsylvania 16802

[§]Department of Mathematics, Purdue University, West Lafayette, Indiana 47907

We proposed a model to study the resistance degradation behavior of ferroelectric oxides in the presence of ferroelectric spontaneous polarization by combining the phase-field model of ferroelectric domains and nonlinear diffusion equations for ionic/electronic transport. We took into account the nonperiodic boundary conditions for solving the electrochemical transport equations and Ginzburg–Landau equations using the Chebyshev collocation algorithm. We considered a single domain structure relative to a thin film BaTiO₃ single crystal orientated to the normal of the electrode plates (Ni) in a single parallel plate capacitor configuration. The capacitor was subjected to a dc bias of 0.5 V either along the polarization direction or opposite to the polarization direction at 25°C. It is shown that the polarization bound charges at the metal/ferroelectric interface play an important role in charge carrier transport and leakage current evolution in BaTiO₃ capacitor.

I. Introduction

FERROELECTRIC perovskites such as barium titanate (BaTiO₃) have become essential materials in various electronic devices such as positive temperature resistors, tunable microwave dielectrics, piezoelectric actuators/sensors, and multilayer ceramic capacitors (MLCCs).¹ Improving the reliability of ceramic capacitors emerges as a critical challenge when operation continues under a continuous bias. Among all the factors affecting the reliability of MLCCs, the long-term resistance degradation is one of the most important. It is characterized by slowly increasing leakage currents under constant voltage stress, which eventually leads to the breakdown of the capacitors.

Two major concerns about the resistance degradation phenomenon are: (1) What are the major reasons that result in the degradation and (2) What is the life time (reliability) of the capacitor. The first problem has been approached by a variety of experimental methods such as the impedance spectroscopy (IS) and thermal simulated depolarization current (TSDC).^{2–12} It is well recognized that the electromigration of oxygen vacancies toward cathode under dc bias is important to the resistance degradation, as is evidenced by the electrocoloration at the anode and cathode.^{2,3} By using impedance spectroscopy (IS) and electron energy loss spectroscopy (EELS), Yang *et al.*⁴ directly observed the oxygen vacancy segregation in BaTiO₃-based ceramic capacitor near the cathode, and oxygen vacancy pile-up at the cathode side within each grain. Yoon *et al.*^{5–9} investigated the effect of acceptor (Mg) concentration on resistance degradation behavior in

acceptor-doped BaTiO₃ ceramic capacitor. He pointed out that the increase in Mg concentration result in higher degradation rates due to the increase in oxygen vacancies. Liu *et al.*^{10,11} carried out TSDC measurement on Fe-doped SrTiO₃ single crystals and ceramics. It was found out that the TSDC peaks associated with the defect dipole, trapped charge, and oxygen vacancy motion are all influenced through degradation process. Liu also studied the charge carriers in degraded SrTiO₃ using IS and EELS and suggested polaron conduction is induced at the cathode as a possible mechanism controlling the insulation transport process and ultimately describing the degradation behavior.¹² Despite all these investigations, however, due to the complexity of multiple factors influencing the degradation, such as acceptor doping concentration, depolarization current, dielectric layer thickness, grain size, conductivity dependence on phase (ferroelectric and paraelectric), nonlinear conduction, electrode roughness, and grain microstructure (grain size, core-shell microstructure), the interdependence and relative importance is not yet fully understood.

In this investigation we theoretically address the degradation kinetics in relation to ferroelectric phase and the role of spontaneous polarization. Typically there is an engineering approach to accessing statistical estimates of the failure times, and the data for this are collected through highly accelerated lifetime tests (HALTS).^{13–15} This method access the time evolution of the electronic conduction under a dc voltage at various temperatures, and the long-term reliability is evaluated using the Eyring model. The testing is often done in the paraelectric phase, and estimated times for failures are extrapolated into the ferroelectric phase which in reality is the operating condition of the capacitors. Such an assumption ignores the role of complex domain structures, the associated electrostrictive and piezoelectric-induced strains that may have influence on the degradation kinetics. Lacking the ferroelectric contributions to the degradation mechanisms, the empirical extrapolations from HALTs measured lifetimes in the paraelectric state may not be representative of the ferroelectric-based capacitors working in their ferroelectric phases.

On the other hand, mathematical models of ionic/electronic defect transport have been proposed to study current response and resistance degradation phenomenon.^{16–27} Baiatu and Waser *et al.* presented classic mathematic models in both SrTiO₃ single crystal and ceramics under high-field stress.^{16,17} In these models the dielectric breakdown is mainly attributed to the electronic compensation for oxygen vacancies accumulation near cathode ($n \approx 2[V_{\text{O}}^{\bullet\bullet}]$, n and $[V_{\text{O}}^{\bullet\bullet}]$ are the electron and oxygen vacancy concentration.) Later Meyer *et al.*¹⁸ suggested pinning of compensating electrons by the work function of the electrodes on both sides of Ba_{0.3}Sr_{0.7}TiO₃ thin film and did not observe any resistance degradation behavior. Strukov *et al.*¹⁹ provided a model of coupled drift-diffusion equations for electrons and ions and examined the mobile ion distributions and current–voltage characteristics of thin film

David Johnson—contributing editor

Manuscript No. 34701. Received March 18, 2014; approved June 30, 2014.

[†]Author to whom correspondence should be addressed. e-mail: yxc238@psu.edu

semiconductor memristive. However, these models do not take into account the effect of ferroelectric polarization on defect transport and current evolution. On the other hand, Xiao and Suryanarayana *et al.* proposed several models which incorporated the semiconducting properties of the wide band-gap ferroelectric perovskites by taking into account the interaction between space charges and polarization.^{20–23} Most recently the charged domain walls are theoretically studied, and the electron and hole response to the polarization bound charge near the domain wall have been calculated.^{24–27} Nevertheless, these models are either limited to the equilibrium profiles or subject to analytical approximation.

In this work, we developed a phase-field model to study the resistance degradation phenomenon in the presence of ferroelectric polarization in ideal ferroelectric capacitor structures. The phase-field approach has been extensively used to study the ferroelectric domain structures in both bulk systems and thin films.^{28–32} The phase-field simulation is based on the time-dependent Ginzburg–Landau (TDGL) equation. We propose to solve the set of electrochemical transport equations using spectral method based on the Chebyshev transforms along the transport direction and Fourier transforms along the plane normal to the transport direction. They are discussed in Section III.

II. Model

In the phase-field simulation, we choose the spontaneous polarization $P_i = (P_1, P_2, P_3)$ as the order parameter to describe the domain structures in ferroelectrics. The total free energy of the system can be expressed as

$$F = \int_V [f_{\text{lan}}(P_i) + f_{\text{grad}}(P_{i,j}) + f_{\text{elas}}(P_i, \epsilon_{ij}) + f_{\text{elec}}(P_i, E_i)] dV, \quad (1)$$

where V is the system volume and $f_{\text{lan}}(P_i)$, $f_{\text{grad}}(P_{i,j})$, $f_{\text{elas}}(P_i, \epsilon_{ij})$, and $f_{\text{elec}}(P_i, E_i)$ are the Landau–Devonshire free energy density, the gradient energy density, elastic energy density, and the electrostatic energy density, respectively. The Landau–Devonshire free energy is written as a polynomial expansion of the polarization components P_i . For an eighth-order expansion under mechanical stress-free boundary condition, it is³²

$$\begin{aligned} f_{\text{lan}} = & \alpha_1 (P_1^2 + P_2^2 + P_3^2) + \alpha_{11} (P_1^4 + P_2^4 + P_3^4) + \alpha_{12} (P_1^2 P_2^2 + P_2^2 P_3^2 + P_3^2 P_1^2) \\ & + \alpha_{111} (P_1^6 + P_2^6 + P_3^6) + \alpha_{112} [P_1^2 (P_2^4 + P_3^4) + P_2^2 (P_1^4 + P_3^4) + P_3^2 (P_1^4 + P_2^4)] \\ & + \alpha_{123} P_1^2 P_2^2 P_3^2 + \alpha_{1111} (P_1^8 + P_2^8 + P_3^8) + \alpha_{1112} [P_1^6 (P_2^2 + P_3^2) + P_2^6 (P_1^2 + P_3^2) + P_3^6 (P_1^2 + P_2^2)] \\ & + \alpha_{1122} (P_1^4 P_2^4 + P_2^4 P_3^4 + P_3^4 P_1^4) + \alpha_{1123} (P_1^4 P_2^2 P_3^2 + P_2^4 P_3^2 P_1^2 + P_3^4 P_1^2 P_2^2) \end{aligned} \quad (2)$$

in which α_{ij} , α_{ijk} , and α_{ijkl} are the fourth, sixth, and eighth-order coefficients, respectively, and the second-order coefficient α_1 is linearly proportional to temperature and obeys the Curie–Weiss law. The Landau coefficients and Curie temperature T_c are here not considered in relation to oxygen stoichiometry.³³ The gradient energy is introduced through the gradients of the polarization ($P_{i,j} = \partial P_i / \partial x_j$). For a general anisotropic system, the gradient energy density is calculated by

$$f_{\text{grad}}(P_{i,j}) = \frac{1}{2} G_{ijkl} P_{i,j} P_{k,l}, \quad (3)$$

in which G_{ijkl} is the gradient energy coefficient. The elastic energy density f_{elas} is given by

$$f_{\text{elas}} = \frac{1}{2} C_{ijkl} e_{ij} e_{kl} = \frac{1}{2} C_{ijkl} (\epsilon_{ij} - \epsilon_{ij}^0) (\epsilon_{kl} - \epsilon_{kl}^0), \quad (4)$$

where C_{ijkl} is the elastic stiffness tensor, ϵ_{ij}^0 is the eigenstrain induced by the spontaneous polarization P_i (the eigenstrain induced by the defect segregation is currently not taken into consideration), and ϵ_{ij} is the total strain of the bulk compared to the parent paraelectric phase. The elastic strain e_{ij} is calculated from $e_{ij} = \epsilon_{ij} - \epsilon_{ij}^0$. Detailed calculation of the eigenstrain and the total strain are described in reference [30]. To consider the dipole–dipole interaction during ferroelectric domain evolution, the electrostatic energy of a domain structure is introduced through

$$f_{\text{elec}} = f(E_i, P_i) = -\frac{1}{2} \epsilon_0 \epsilon_r E_i E_j - E_i P_i, \quad (5)$$

where E_i is the electric field component, ϵ_0 and ϵ_r are the vacuum permittivity and dielectric constant of the material, respectively.

Based on the Landau–Devonshire free energy density, the gradient energy density, elastic energy density, and the electrostatic energy density calculated from Eqs. (2) to (5), the total free energy F is obtained from Eq. (1). The temporal evolution of order parameter P are governed by the TDGL equations

$$\frac{\partial P_i(x, t)}{\partial t} = -L \frac{\delta F}{\delta P_i(x, t)}, \quad i = 1, 2, 3, \quad (6)$$

where L is the kinetic coefficient which is related to the domain movement and t is time.

The local electric field in Eq. (5) is dependent on the space charges as well as the polarization-induced bound charges. It also depends on the boundary conditions on the film surfaces. The local electric field/potential distribution is governed by the Poisson equation

$$-\nabla^2 \psi = \frac{\rho - \nabla \cdot P_i}{\epsilon_0 \epsilon_r} = \frac{q_0 (2[V_{\text{O}}^{\bullet\bullet}] + p - n - [A']) - \nabla \cdot P_i}{\epsilon_0 \epsilon_r}, \quad (7)$$

in which ψ is the local electric potential, ρ is the total space charge density, q_0 is the unit charge, $[V_{\text{O}}^{\bullet\bullet}]$, n , p , and $[A']$

denote the local concentrations of oxygen vacancy, electron, hole, and ionized acceptor, respectively. The polarization-induced charges are introduced by $-\nabla \cdot P$. The electric field E is related to the electric potential through

$$\vec{E} = -\nabla \psi. \quad (8)$$

The boundary condition for the electric potential is defined as

$$\psi|_{z=0} = V_a(0), \quad \psi|_{z=L} = V_a(L), \quad (9)$$

in which $V_a(0)$ and $V_a(L)$ are specified from the externally applied potential bias at $z = 0, L$.

The bulk transports of space charges in Eq. (7) are described by the diffusion equations with proper boundary conditions. In our current simulation, the major charged defects of interest include the oxygen vacancies ($V_{\text{O}}^{\bullet\bullet}$), electrons (e'), holes (h'), ionized acceptors (A') written in Kröger–Vink notation.³⁴ The oxygen vacancies, electrons, and holes are considered as mobile species. The monovalent acceptors are introduced from the substitution of +3 elements such as Fe and Al on the Ti sites (Fe'_{Ti} and $\text{Al}'_{\text{Ti}} = A'$) and are considered fully ionized and immobile.

Due to extreme low mobility compared to electrons and holes, oxygen vacancies are considered to be the major factors in determining the simulation time. The oxygen vacancy migration consists of the chemical diffusion due to concentration gradient and the electrical drift under the external applied electric field. Here, we do not consider the presence of association and the formation of defect dipoles. A nonlinear Nernst–Planck transport model is applied to describe the oxygen vacancy migration,^{35,36}

$$\begin{aligned} J_{V_{\text{O}}^{\bullet\bullet}} &= -D_{V_{\text{O}}^{\bullet\bullet}} \nabla [V_{\text{O}}^{\bullet\bullet}] - \mu_{V_{\text{O}}^{\bullet\bullet}} [V_{\text{O}}^{\bullet\bullet}] \frac{2k_{\text{B}}T}{z_{V_{\text{O}}^{\bullet\bullet}} q_0 \Delta \vec{x}} \sinh\left(\frac{z_{V_{\text{O}}^{\bullet\bullet}} q_0 \Delta \phi_{12}}{2k_{\text{B}}T}\right) \\ \frac{\partial [V_{\text{O}}^{\bullet\bullet}]}{\partial t} &= -\nabla \cdot J_{V_{\text{O}}^{\bullet\bullet}} = D_{V_{\text{O}}^{\bullet\bullet}} \nabla^2 [V_{\text{O}}^{\bullet\bullet}] + \mu_{V_{\text{O}}^{\bullet\bullet}} \frac{2k_{\text{B}}T}{z_{V_{\text{O}}^{\bullet\bullet}} q_0 \Delta \vec{x}} \nabla \cdot \left([V_{\text{O}}^{\bullet\bullet}] \sinh\left(\frac{z_{V_{\text{O}}^{\bullet\bullet}} q_0 \Delta \phi_{12}}{2k_{\text{B}}T}\right) \right) \end{aligned} \quad (10)$$

in which $[V_{\text{O}}^{\bullet\bullet}]$ is the oxygen vacancy concentration, $J_{V_{\text{O}}^{\bullet\bullet}}$ is the flux of the oxygen vacancy, $D_{V_{\text{O}}^{\bullet\bullet}}$ and $\mu_{V_{\text{O}}^{\bullet\bullet}}$ are the diffusivity and mobility of oxygen vacancy, respectively, which are related with each other through the Nernst–Einstein equation

$$D_{V_{\text{O}}^{\bullet\bullet}} = \frac{k_{\text{B}}T}{z_{V_{\text{O}}^{\bullet\bullet}} q_0} \mu_{V_{\text{O}}^{\bullet\bullet}}, \quad (11)$$

k_{B} is the Boltzmann constant, T is the absolute temperature, $z_{V_{\text{O}}^{\bullet\bullet}} = +2$ denotes the charge number of oxygen vacancy, and q_0 is the unit charge. $\Delta \phi_{12}$ and $\Delta \vec{x}$ are the electric potential difference and distance between two adjacent grid points, respectively.

The Ni electrodes act as the blocking boundaries for oxygen vacancies migration during the resistance degradation so that the boundary condition for Eq. (10) can be written as

$$J_{V_{\text{O}}^{\bullet\bullet}} \Big|_{z=0,L} = 0. \quad (12)$$

On the other hand, electrons and holes are moving much faster than oxygen vacancies due to their higher mobility. In our simulations we assumed that the electron and hole concentrations always reach equilibrium for each evolution of oxygen vacancy profile. Mathematically we solve steady-state equations for electron and hole transports assuming $\partial n / \partial t = 0$ and $\partial p / \partial t = 0$

$$\begin{aligned} J_{\text{n}} &= -D_{\text{n}} \nabla n - \mu_{\text{n}} n \vec{E} \\ \frac{\partial n}{\partial t} &= -\nabla \cdot J_{\text{n}} = D_{\text{n}} \nabla^2 n + \mu_{\text{n}} \nabla \cdot [n \vec{E}] = 0 \end{aligned} \quad (13)$$

$$\begin{aligned} J_{\text{p}} &= -D_{\text{p}} \nabla p + \mu_{\text{p}} p \vec{E} \\ \frac{\partial p}{\partial t} &= -\nabla \cdot J_{\text{p}} = D_{\text{p}} \nabla^2 p - \mu_{\text{p}} \nabla \cdot [p \vec{E}] = 0 \end{aligned} \quad (14)$$

The electron and hole concentrations at the Ni/BaTiO₃ interface are pinned by the Ni electrode as

$$n_{z=0,L} = N_{\text{c}} \exp\left(-\frac{E_{\text{c}} - E_{\text{fm}}}{k_{\text{B}}T}\right) \quad (15)$$

$$p_{z=0,L} = N_{\text{v}} \exp\left(-\frac{E_{\text{fm}} - E_{\text{v}}}{k_{\text{B}}T}\right), \quad (16)$$

in which N_{c} and N_{v} are the effective density of states of the conduction band and valance band, respectively. E_{c} and E_{v} are the energy of the conduction band minimum and valance band maximum of BaTiO₃, respectively. E_{fm} is the work function of Ni plate electrode.

The current density is contributed from the flow of the charged species including oxygen vacancies, electrons, and holes. The current density for particular charged carrier i and the total current density are given by

$$I_i = q_0 z_i J_i, \quad i = V_{\text{O}}^{\bullet\bullet}, e', p' \quad (17)$$

$$I_{\text{total}} = \sum_i I_i, \quad (18)$$

in which z_i and J_i denote the charge number and the flux of each of the charge species.

III. Results and Discussions

We first consider an ideal situation regarding the influence of a high spontaneous polarization on the transport processes. We consider a single tetragonal domain structure, such as a thin film BaTiO₃ single crystal orientated normal to the electrode plates (Ni) in a single parallel plate capacitor configuration. We set up a coordinate system with a periodic boundary condition along x and y directions. Along z direction it is nonperiodic so that a Chebyshev collocation boundary condition is applied. We are mainly concerned with the ionic/electronic transport along z direction, and the polarization direction is also assumed to be along z direction. Therefore, the system size of the simulation is chosen to be $1 \times 1 \times 200$. The temporal evolution of the polarization field and thus the domain structures are obtained by numerically solving the TDGL equations using the semi-implicit Fourier spectral method.^{37–40} The corresponding material constants for the Landau free energy, the gradient energy coefficients, the electrostrictive coefficients, and elastic properties are taken from the literature.^{32,41} The parameters used in the simulation are listed in Table I.

We started with a charge neutral single tetragonal domain BaTiO₃ of thickness $L = 500$ nm constrained by Ni plate electrodes on two sides at room temperature (25°C). The acceptor doping concentration was $[A'] = 2.0 \times 10^{18} \text{ cm}^{-3}$. All the ionic and electronic defects were assumed to be homogeneously distributed and the local charge neutrality condition was maintained in the initial state

$$2[V_{\text{O}}^{\bullet\bullet}] + p - n - [A'] = 0. \quad (19)$$

The initial polarization was assumed to be homogeneous and equal to the spontaneous polarization $P = P_s = 26 \mu\text{C}/$

Table I. Parameters Used in the Simulation

Parameter	Value
Temperature, T (K)	298
Total thickness, L (nm)	500
Dielectric constant, ϵ_r	200
Electron/hole mobility, μ_n, μ_p [$\text{cm}^2 (\text{V}\cdot\text{s})^{-1}$]	0.67, 0.35 ³
Oxygen vacancy mobility, μ_{V_o} [$\text{cm}^2 (\text{V}\cdot\text{s})^{-1}$]	1.0×10^{-14} ³
External bias (V)	0.5
Conduction band, E_c (eV)	-3.6 ⁴⁵
Valence band, E_v (eV)	-6.7 ⁴⁵
Work function of Ni electrode, E_{fm} (eV)	-5.2 ⁴⁵
Effective density of states, N_c, N_v (cm^{-3})	10^{22}

cm^2 which was oriented along the $+z$ direction. The boundary condition of polarization at the metal/ferroelectric interface in 1D was specified as

$$a \times P - b \times \frac{dP}{dz} \Big|_{z=0} = 0, \quad a \times P + b \times \frac{dP}{dz} \Big|_{z=L} = 0, \quad (20)$$

where coefficients a and b were chosen to be 1.0 and 0.05 cm, respectively, representing a partially compensated boundary condition.

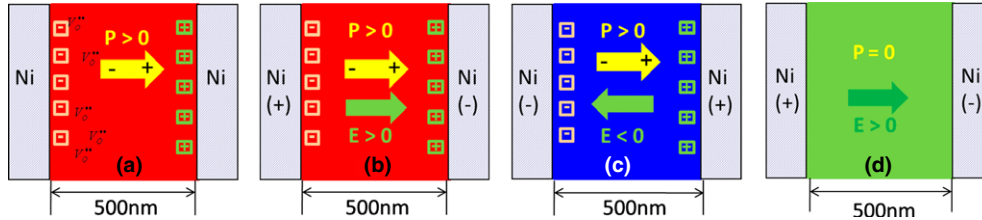


Fig. 1. Schematic plot of the metal (Ni)/ferroelectric (BaTiO₃)/metal (Ni) sandwich structure: (a) without bias; (b) under applied bias in the same direction of polarization; (c) under applied bias in the reverse direction of polarization; (d) under applied bias without ferroelectric spontaneous polarization. The yellow and green arrows denote the directions of polarization and electric field, respectively. The (+) and (-) signs represent the anode and cathode, respectively. The \square and \boxplus signs denote the polarization bound charge near the metal/ferroelectric interfaces.

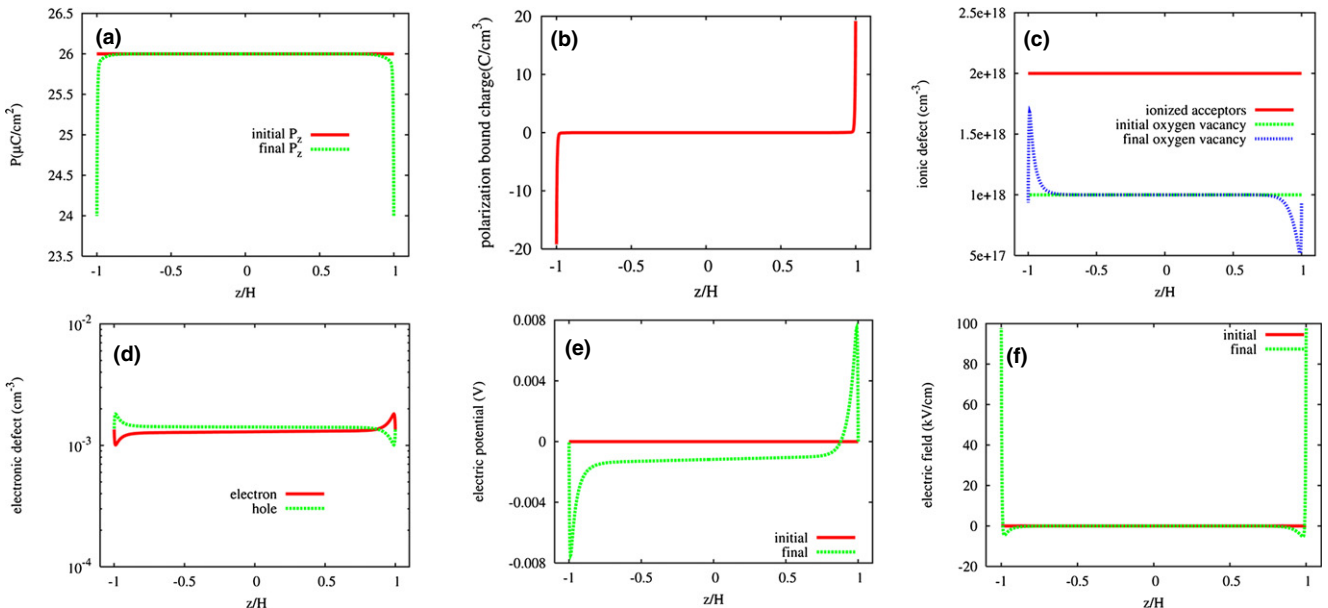


Fig. 2. Equilibrium profile of single domain BaTiO₃ without bias: (a) polarization (P_z), (b) polarization bound charge ($-dP_z/dz$), (c) ionic defects (d) electronic defects, (e) electric potential, and (f) electric field (z denotes the position in the film, $H = 250$ nm is half of the film thickness L , so that z/H from -1 to $+1$ represents the entire thin film thickness).

The simulation was then performed at $T = 25^\circ\text{C}$ until defect and polarization distributions reached steady state under no external bias, which are schematically plotted in Fig. 1(a). The equilibrium profiles are shown in Fig. 2. From Fig. 2(a) it is seen that the ferroelectric polarization remained constant inside the bulk BaTiO₃ and decreased at the metal/ferroelectric interfaces. As a result, a sheet of positive bound charge was formed at one interface ($z/H = +1$) and a negative bound charge on the other ($z/H = -1$) [Fig. 2(b)]. For charge compensation, the positively charged oxygen vacancies and holes tended to segregate at $z/H = -1$, while the negatively charged electrons at $z/H = +1$ [Figs. 2(c) and (d)]. It should be noted that the electronic concentrations are much lower than oxygen vacancies. This is because of the wide band gap (~ 3.1 eV) of BaTiO₃.⁴² In response to the redistribution of polarization bound charges and the ionic/electronic space charges, the local electric potential and electric field were obtained from Eqs. (7) and (8) under the short circuit boundary condition $V_a|_{z=-H} = V_a|_{z=H} = 0$ [Figs. 2(e) and (f)]. A large positive electric field was formed at the metal/ferroelectric interfaces due to electric potential to be 0 at the boundaries.

When the equilibrium profile was reached, the resistance degradation simulations were carried out by applying a dc bias of 0.5 V along the polarization direction ($+z$ direction). Under the field stress, the oxygen vacancies were migrating toward the cathode side ($z/H = +1$) [Fig. 3(a)], resulting in a positive ionic charge region at $z/H = +1$ and a negative ionic charge region at $z/H = -1$, given that ionized acceptors are immobile. In response to the local ionic charges, the electrons

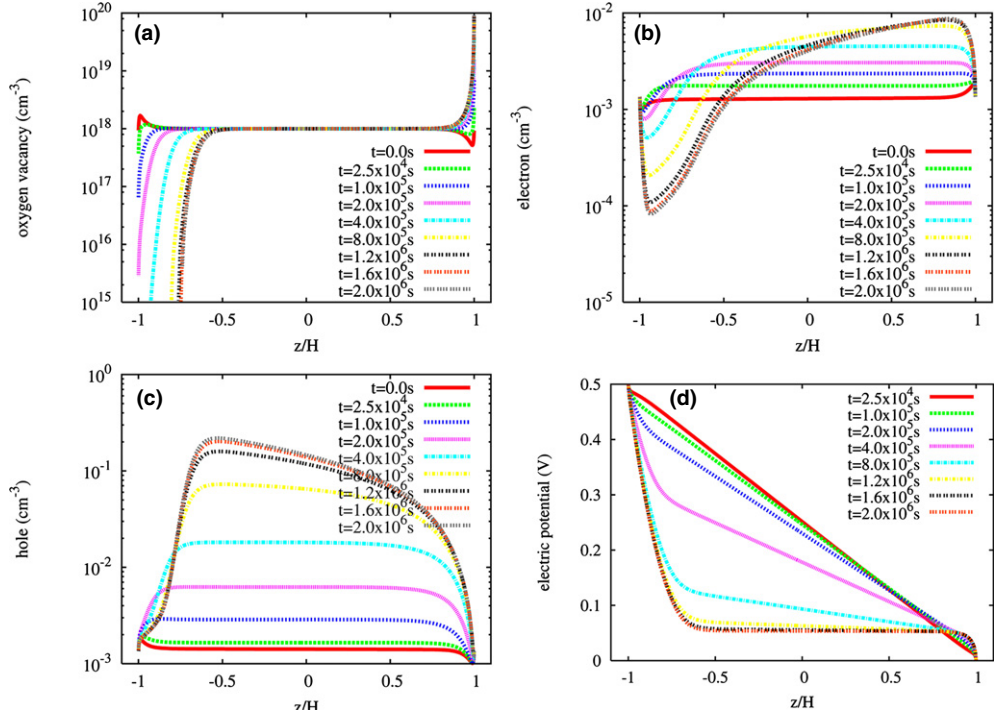


Fig. 3. Defect transport and electric potential evolution in single domain BaTiO₃ plate capacitor at $T = 25^\circ\text{C}$ under dc bias (0.5 V) along $+z$ direction (a) oxygen vacancies, (b) electrons, (c) holes, and (d) electric potential evolution.

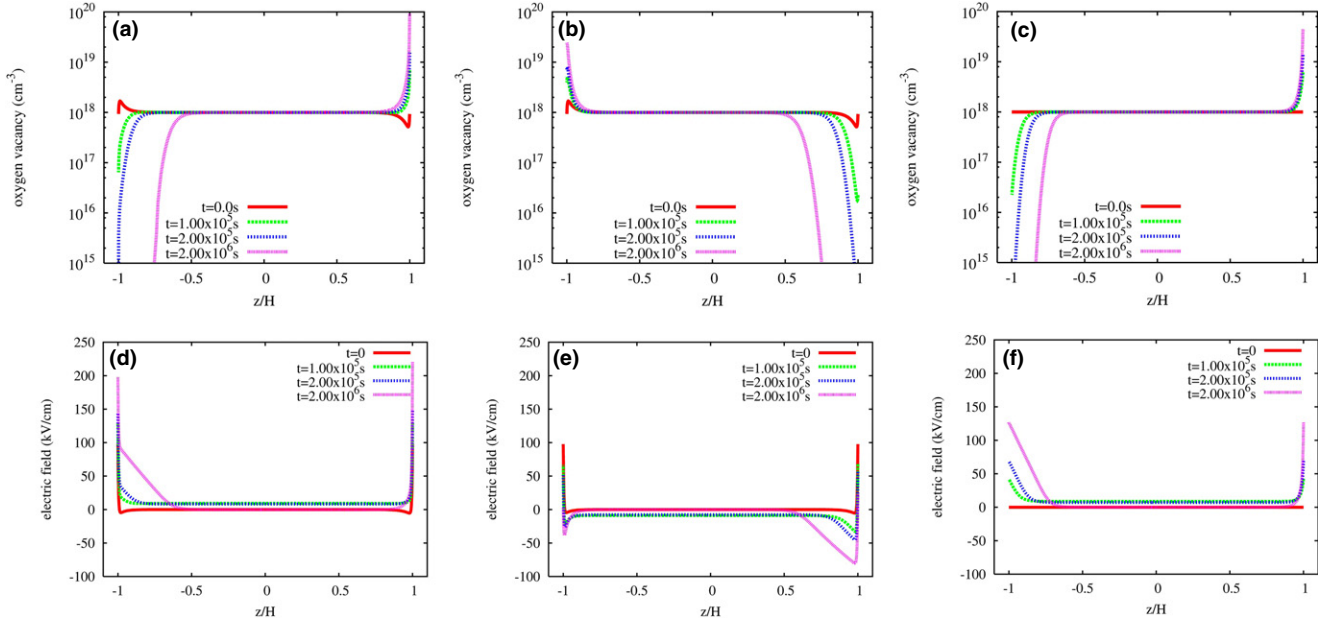


Fig. 4. Comparison of oxygen vacancy evolution (a–c) and local electric field (d–f) distribution in single crystal BaTiO₃ plate capacitor subjected to 0.5 V at $T = 25^\circ\text{C}$ (a) and (d): applied field in the same direction of polarization; (b) and (e): applied field in the opposite direction of polarization; (c) and (f): no polarization.

tended to migrate toward the cathode and holes toward anode [Figs. 3(b) and (c)]. However, the electronic charge compensation was much smaller than the ionic charges since the electronic defects were pinned by the Ni plate electrodes at the boundaries. The electric potential evolution was plotted in Fig. 3(d), in which a large electric potential gradient was formed near the anode side in steady state. This agrees with recent experimental results by Okamoto *et al.*⁴³ in which a large electric field was observed at anode side in the degraded MLCCs. It should be noted that in the current simulation we do not consider the possibility of anodic Ni plate electrode oxidation due to the oxygen vacancy depletion/

oxygen ion accumulation under long-term bias in the current simulation, which could change the capacitance value.

We also applied a dc bias of 0.5 V in the opposite direction of the polarization ($-z$ direction). The reverse bias was small enough so that the single domain was not allowed to switch. For comparison we also considered the situation when there is no spontaneous polarization. Figures 1(b)–(d) schematically illustrates three different situations of BaTiO₃ single plate capacitor subject to dc biases. The oxygen vacancy evolutions were plotted in Figs. 4(a)–(c). In all three cases, the oxygen vacancies tended to migrate along the applied field direction. However, the oxygen vacancy

segregation reached $\sim 10^{20} \text{ cm}^{-3}$ along the cathode side when the field was along the polarization direction [Fig. 4(a)], it reached only $\sim 2.5 \times 10^{19} \text{ cm}^{-3}$ when the field was opposite to the polarization direction [Fig. 4(b)] and $\sim 4.4 \times 10^{19} \text{ cm}^{-3}$ when there was no polarization [Fig. 4(c)]. A possible explanation for the difference is that the polarization promotes the ionic transport and further deteriorates the resistance of the capacitor when it is along the field direction. Note these concentrations are close to the Mott Criterion, and in the ferroelectric state are expected to be semiconducting.⁴⁴ To further understand the differences of oxygen vacancy segregation among three situations, we investigated the electric field distribution inside the BaTiO₃ dielectric layers [Figs. 4(d)–(f)]. From Fig. 2(f), positive electric fields were seen at Ni/BaTiO₃ interfaces without applied field. When a positive external bias was applied on BaTiO₃, the local fields at the boundaries was enhanced to 200 kV/cm [Fig. 4(d)], which acted as a large driving force for the oxygen vacancy migration along the +z direction. Under negative bias, the field became negative inside the BaTiO₃ layer leading to the oxygen vacancies migration along -z direction. However, at the interfacial regions, the local field still remained positive ($\sim 50 \text{ kV/cm}$) at $\sim 10^5 \text{ s}$ [Fig. 4(e)], thus inhibited the further migration of oxygen vacancy toward cathode. When the ferroelectric polarization was zero, the local electric field at the interfaces reached $\sim 120 \text{ kV/cm}$ [Fig. 4(f)]. Therefore, the amount of oxygen vacancy segregation with $P = 0$ lied between the other two cases.

The current density evolutions were compared among the aforementioned three cases (Fig. 5). The leakage currents all experienced small and slow increases in the initial state when the oxygen vacancies started to migrate under the external biases, followed by fast and significant increases indicating the breakdown of the capacitor. The rapid leakage current increase could be attributed to the oxygen vacancy segregation and the local field concentration in cathodes. The leakage current with $P = 0$ increased about one order of magnitude, and was remarkably enhanced ($\sim 40\times$) under positive bias and inhibited ($\sim 5\times$) under negative bias. This agrees with the evolution of oxygen vacancies and local fields shown in Fig. 4. It should also be noted that the current underwent an observable decrease before $t = 10^5 \text{ s}$ under negative bias (blue line in Fig. 5). This is because of the electric current along +z direction due to the positive local field at cathode region [Fig. 4(e)], which offset the negative current along -z direction inside the bulk BaTiO₃. When $t > 10^5 \text{ s}$, the local field at cathode further decreased to negative (blue line in Fig. 5) so that the total current along -z

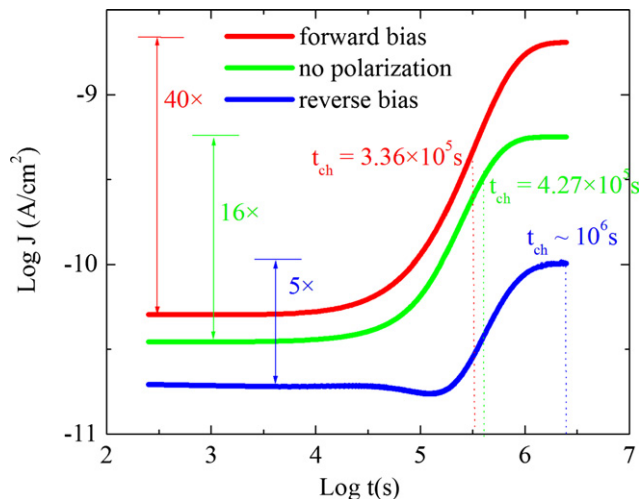


Fig. 5. Leakage current evolution of BaTiO₃ single parallel layer capacitor under forward bias, reverse bias, and no polarization at 25°C.

direction increased. On the other hand, we also compared the mean time to failure (MTTF) among the three cases. The MTTF was determined as the leakage current increases one decade above its minimum value. From Figs. 4 and 5, it is evident that the ferroelectric polarization accelerates the oxygen vacancy migration, promotes the net leakage current increase and decreases the MTTF when it is along the applied field direction.

The electric field dependence of MTTF was plotted for all three cases in Fig. 6(a). While the $\log(\text{MTTF})$ versus $\log(\text{field})$ curves exhibit almost linear relation at small field region, a nonlinear field dependence of MTTF is clearly seen at large field region for all the three cases [Fig. 6(a)]. This nonlinear dependence of current on electric field has been reported by Riess *et al.*^{35,36} More recently, Randall *et al.*¹⁵ suggested a ion conduction model to describe the transfer of oxygen vacancies and used it to account for MTTF data

$$j = 2q_0 N a v \exp\left(-\frac{U}{k_B T}\right) \sinh\left(\frac{q_0 E a}{2k_B T}\right), \quad (21)$$

in which j is the current, N is the number of ion, a is the distance of ion hopping, v is the frequency of ion, U is the activation energy dependent mainly on temperature, and E is the applied electric field strength. The life time of capacitor can

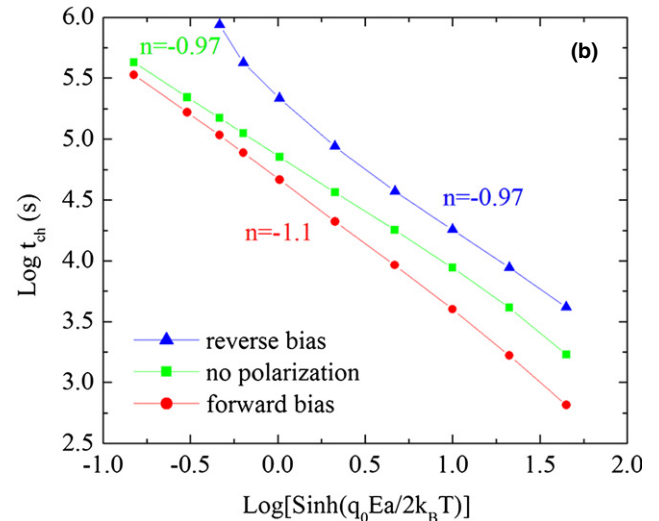
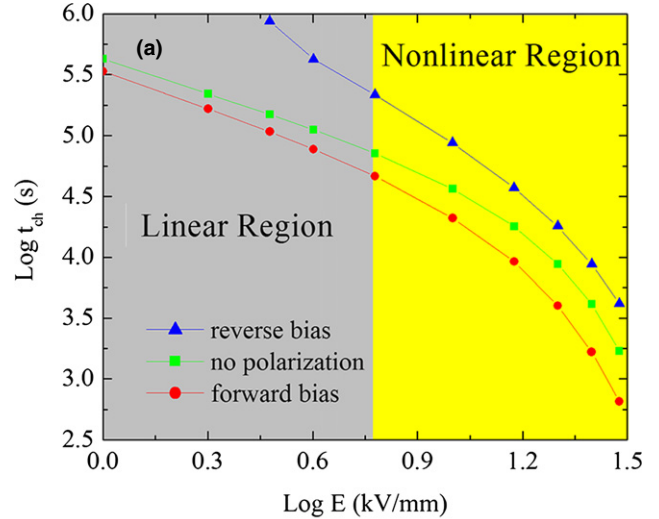


Fig. 6. Electric field strength dependence of mean time to failure of single plate BaTiO₃ capacitor (a) $\log t_{\text{ch}}$ versus $\log E$, (b) $\log t_{\text{ch}}$ versus $\log\left(\sinh\left(\frac{q_0 E a}{2k_B T}\right)\right)$.

be considered as the time to a certain amount of transport charge accumulation (Q), which is assumed to be constant at different temperature and voltage conditions. As a result, the MTF can be represented as

$$t_{\text{ch}} = Q/j = C \exp\left(-\frac{U}{k_B T}\right) \left(\sinh \frac{q_0 E a}{2k_B T}\right)^{-1} \quad (22)$$

$$\log t_{\text{ch}} = C' - \log\left(\sinh \frac{q_0 E a}{2k_B T}\right)$$

A replot of the field dependence of MTF with $\log t_{\text{ch}}$ versus $\log\left(\sinh \frac{q_0 E a}{2k_B T}\right)$ from our simulation clearly shows linear relations [Fig. 6(b)]. It is found out that the slopes of the curves are -1.1 , -0.97 , and -0.97 for positive bias, negative bias, and no polarization cases, respectively. This agrees well with the phenomenological model proposed by Randall *et al.*¹⁵

IV. Summary

In this paper, we developed a phase-field model combined with nonlinear transport equations to study the resistance degradation behavior of mono-domain BaTiO₃ single plate capacitor. Our results show that the electrochemical migration of oxygen vacancies contributes to the resistance degradation. On the other hand, the ferroelectric polarization modulates the local electric field distribution at the metal/ferroelectric interfaces, promotes the oxygen vacancy segregation and further deteriorates the resistance of the capacitor when it is along the direction of the external applied field. Our simulation result on the nonlinear electric field strength dependence of MTF agrees well with a recently reported ion conduction model. In the future we will further extend the current model to incorporate the multidomain structures and grain structures to study their effect on transport dynamics and degradation behaviors.

Acknowledgments

The authors are grateful to the financial support by the NSF-IUCRC Center for Dielectric Studies at Penn State and the Air Force Office of Scientific Research under the Aerospace Materials for Extreme Environments Program. The work of Jie Shen is partially supported by NSF DMS-1215066 and by the Computational Materials and Chemical Sciences Network (CMCSN).

References

- ¹O. Auciello, J. F. Scott, and R. Ramesh, "The Physics of Ferroelectric Memories," *Phys. Today*, **51** [7] 22–7 (1998).
- ²R. Waser, T. Baiatu, and K. H. Hardtl, "Dc Electrical Degradation of Perovskite-Type Titanates .2. Single-Crystals," *J. Am. Ceram. Soc.*, **73** [6] 1654–62 (1990).
- ³H. I. Yoo, M. W. Chang, T. S. Oh, C. E. Lee, and K. D. Becker, "Electrocoloration and Oxygen Vacancy Mobility of BaTiO₃," *J. Appl. Phys.*, **102**, 093701, 8pp (2007).
- ⁴G. Y. Yang, G. D. Lian, E. C. Dickey, C. A. Randall, D. E. Barber, P. Pinceloup, M. A. Henderson, R. A. Hill, J. J. Beeson, and D. J. Skamser, "Oxygen Nonstoichiometry and Dielectric Evolution of BaTiO₃. Part II—Insulation Resistance Degradation Under Applied dc Bias," *J. Appl. Phys.*, **96** [12] 7500–8 (2004).
- ⁵S. H. Yoon, M. H. Hong, J. O. Hong, Y. T. Kim, and K. H. Hur, "Effect of Acceptor (Mg) Concentration on the Electrical Resistance at Room and High (200 Degrees C) Temperatures of Acceptor (Mg)-Doped BaTiO₃ Ceramics," *J. Appl. Phys.*, **102**, 054105, 9pp (2007).
- ⁶S. H. Yoon, C. A. Randall, and K. H. Hur, "Influence of Grain Size on Impedance Spectra and Resistance Degradation Behavior in Acceptor (Mg)-Doped BaTiO₃ Ceramics," *J. Am. Ceram. Soc.*, **92** [12] 2944–52 (2009).
- ⁷S. H. Yoon, C. A. Randall, and K. H. Hur, "Effect of Acceptor (Mg) Concentration on the Resistance Degradation Behavior in Acceptor (Mg)-Doped BaTiO₃ Bulk Ceramics: II. Thermally Stimulated Depolarization Current Analysis," *J. Am. Ceram. Soc.*, **92** [8] 1766–72 (2009).
- ⁸S. H. Yoon, C. A. Randall, and K. H. Hur, "Correlation Between Resistance Degradation and Thermally Stimulated Depolarization Current in Acceptor (Mg)-Doped BaTiO₃ Submicrometer Fine-Grain Ceramics," *J. Am. Ceram. Soc.*, **93** [7] 1950–6 (2010).

- ⁹S. H. Yoon, S. H. Kwon, and K. H. Hur, "Dielectric Relaxation Behavior of Acceptor (Mg)-Doped BaTiO₃," *J. Appl. Phys.*, **109**, 084117, 8pp (2011).
- ¹⁰W. Liu and C. A. Randall, "Thermally Stimulated Relaxation in Fe-Doped SrTiO₃ Systems: I. Single Crystals," *J. Am. Ceram. Soc.*, **91** [10] 3245–50 (2008).
- ¹¹W. Liu, and C. A. Randall, "Thermally Stimulated Relaxation in Fe-Doped SrTiO₃ Systems: II. Degradation of SrTiO₃ Dielectrics," *J. Am. Ceram. Soc.*, **91** [10] 3251–7 (2008).
- ¹²W. Liu, G. Y. Yang, and C. A. Randall, "Evidence for Increased Polaron Conduction Interface in the Final Stages of Electrical Degradation in SrTiO₃ Crystals," *Jpn. J. Appl. Phys.*, **48**, 051404, 6pp (2009).
- ¹³R. Waser, T. Baiatu, and K. H. Hardtl, "Dc Electrical Degradation of Perovskite-Type Titanates .1. Ceramics," *J. Am. Ceram. Soc.*, **73** [6] 1645–53 (1990).
- ¹⁴S. Zhao, S. J. Zhang, W. Liu, N. J. Donnelly, Z. Xu, and C. A. Randall, "Time Dependent dc Resistance Degradation in Lead-Based Perovskites: 0.7 Pb(Mg(1/3)Nb(2/3))O(3)-0.3 PbTiO₃," *J. Appl. Phys.*, **105**, 053705, 7pp (2009).
- ¹⁵C. A. Randall, R. Maier, W. Qu, K. Kobayashi, K. Morita, Y. Mizuno, N. Inoue, and T. Oguni, "Improved Reliability Predictions in High Permittivity Dielectric Oxide Capacitors Under High dc Electric Fields with Oxygen Vacancy Induced Electromigration," *J. Appl. Phys.*, **113**, 014101, 6pp (2013).
- ¹⁶T. Baiatu, R. Waser, and K. H. Hardtl, "Dc Electrical Degradation of Perovskite-Type Titanates .3. A Model of the Mechanism," *J. Am. Ceram. Soc.*, **73** [6] 1663–73 (1990).
- ¹⁷T. Holbling, N. Soylemezoglu, and R. Waser, "A Mathematical-Physical Model for the Charge Transport in p-Type SrTiO₃ Ceramics Under dc Load: Maxwell-Wagner Relaxation," *J. Electroceram.*, **9** [2] 89–102 (2002).
- ¹⁸R. Meyer, R. Liedtke, and R. Waser, "Oxygen Vacancy Migration and Time-Dependent Leakage Current Behavior of Ba_{0.3}Sr_{0.7}TiO₃ Thin Films," *Appl. Phys. Lett.*, **86**, 112904, 3pp (2005).
- ¹⁹D. B. Strukov, J. L. Borghetti, and R. S. Williams, "Coupled Ionic and Electronic Transport Model of Thin-Film Semiconductor Memristive Behavior," *Small*, **5** [9] 1058–63 (2009).
- ²⁰Y. Xiao and K. Bhattacharya, "Interaction of Oxygen Vacancies with Domain Walls and its Impact on Fatigue in Ferroelectric Thin Films," vol. **5387**, pp. 354–65 in *Proceedings Smart Structures and Materials 2004: Active Materials: Behavior and Mechanics*, (2004).
- ²¹Y. Xiao, V. B. Shenoy, and K. Bhattacharya, "Depletion Layers and Domain Walls in Semiconducting Ferroelectric Thin Films," *Phys. Rev. Lett.*, **95**, 247603, 4pp (2005).
- ²²Y. Xiao and K. Bhattacharya, "A Continuum Theory of Deformable, Semiconducting Ferroelectrics," *Arch. Ration. Mech. Anal.*, **189** [1] 59–95 (2008).
- ²³P. Suryanarayana and K. Bhattacharya, "Evolution of Polarization and Space Charges in Semiconducting Ferroelectrics," *J. Appl. Phys.*, **111**, 034109, 11pp (2012).
- ²⁴A. K. Tagantsev and G. Gerra, "Interface-Induced Phenomena in Polarization Response of Ferroelectric Thin Films," *J. Appl. Phys.*, **100**, 051607, 28pp (2006).
- ²⁵M. Y. Gureev, A. K. Tagantsev, and N. Setter, "Head-to-Head and Tail-to-Tail 180 Degrees Domain Walls in an Isolated Ferroelectric," *Phys. Rev. B*, **83**, 184104, 18pp (2011).
- ²⁶E. A. Eliseev, A. N. Morozovska, G. S. Svechnikov, V. Gopalan, and V. Y. Shur, "Static Conductivity of Charged Domain Walls in Uniaxial Ferroelectric Semiconductors," *Phys. Rev. B*, **83**, 235313, 8pp (2011).
- ²⁷T. Sluka, A. K. Tagantsev, D. Damjanovic, M. Gureev, and N. Setter, "Enhanced Electromechanical Response of Ferroelectrics due to Charged Domain Walls," *Nat. Commun.*, **3**, 748, 7pp (2012).
- ²⁸H. L. Hu, and L. Q. Chen, "Computer Simulation of 90 Degrees Ferroelectric Domain Formation in Two-Dimensions," *Mater. Sci. Eng. A Struct. Mater.*, **238** [1] 182–91 (1997).
- ²⁹Y. L. Li, S. Y. Hu, Z. K. Liu, and L. Q. Chen, "Phase-Field Model of Domain Structures in Ferroelectric Thin Films," *Appl. Phys. Lett.*, **78** [24] 3878–80 (2001).
- ³⁰Y. L. Li, S. Y. Hu, Z. K. Liu, and L. Q. Chen, "Effect of Substrate Constraint on the Stability and Evolution of Ferroelectric Domain Structures in Thin Films," *Acta Mater.*, **50** [2] 395–411 (2002).
- ³¹Y. L. Li, L. Q. Chen, G. Asayama, D. G. Schlom, M. A. Zurbuchen, and S. K. Streiffner, "Ferroelectric Domain Structures in SrBi₂Nb₂O₉ Epitaxial Thin Films: Electron Microscopy and Phase-Field Simulations," *J. Appl. Phys.*, **95** [11] 6332–40 (2004).
- ³²Y. L. Li, L. E. Cross, and L. Q. Chen, "A Phenomenological Thermodynamic Potential for BaTiO₃ Single Crystals," *J. Appl. Phys.*, **98**, 064101, 4pp (2005).
- ³³S. Lee, G. A. Rossetti, Z. K. Liu, and C. A. Randall, "Intrinsic Ferroelectric Properties of the Nonstoichiometric Perovskite Oxide Ba_{1-x}Ti_{1-y}O_{3-x-2y}," *J. Appl. Phys.*, **105**, 093519, 6pp (2009).
- ³⁴F. A. Kroger and H. J. Vink, "Relations Between the Concentrations of Imperfections in Crystalline Solids," *Solid State Phys.*, **3**, 307–435 (1956).
- ³⁵I. Riess and J. Maier, "Symmetrized General Hopping Current Equation," *Phys. Rev. Lett.*, **100**, 205901, 4pp (2008).
- ³⁶I. Riess and J. Maier, "Current Equation for Hopping Ions on a Lattice Under High Driving Force and Nondilute Concentration," *J. Electrochem. Soc.*, **156** [1] P7–20 (2009).
- ³⁷Y. Cao, S. Bhattacharya, J. Shen, C. A. Randall, and L. Q. Chen, "Role of Polaron Hopping in Leakage Current Behavior of a SrTiO₃ Single Crystal," *J. Appl. Phys.*, **114**, 224102, 7pp (2013).

³⁸L. Q. Chen and J. Shen, "Applications of Semi-Implicit Fourier-Spectral Method to Phase Field Equations," *Comput. Phys. Commun.*, **108** [2–3] 147–58 (1998).

³⁹J. Shen and T. Tang, *Spectral and High-Order Methods with Applications*. Chinese Science Press, Beijing, China, 2006.

⁴⁰J. Shen, T. Tang, and L. L. Wang, *Spectral Methods: Algorithms, Analysis and Applications*. Springer, Berlin, Germany, 2011.

⁴¹G. Sheng, J. X. Zhang, Y. L. Li, S. Choudhury, Q. X. Jia, Z. K. Liu, and L. Q. Chen, "Misfit Strain-Misfit Strain Diagram of Epitaxial BaTiO₃ Thin Films: Thermodynamic Calculations and Phase-Field Simulations," *Appl. Phys. Lett.*, **93**, 232904, 3pp (2008).

⁴²S. Lee, W. H. Woodford, and C. A. Randall, "Crystal and Defect Chemistry Influences on Band Gap Trends in Alkaline Earth Perovskites," *Appl. Phys. Lett.*, **92**, 201909, 3pp (2008).

⁴³T. Okamoto, S. Kitagawa, N. Inoue, and A. Ando, "Electric Field Concentration in the Vicinity of the Interface Between Anode and Degraded BaTiO₃-Based Ceramics in Multilayer Ceramic Capacitor," *Appl. Phys. Lett.*, **98**, 072905, 3pp (2011).

⁴⁴S. Lee, J. A. Bock, S. Trolier-McKinstry, and C. A. Randall, "Ferroelectric-Thermoelectricity and Mott Transition of Ferroelectric Oxides with High Electronic Conductivity," *J. Eur. Ceram. Soc.*, **32** [16] 3971–88 (2012).

⁴⁵J. F. Scott, *Ferroelectric Memories*. Springer, Berlin, Germany, 2000. □